Available online at www.sciencedirect.com
SCIENCE DIRECT®
Journal of Theoretical Biology 231 (2004) 153–166
Journal of Theoretical Biology
www.elsevier.com/locate/yjtbi

The role of virus infection in a simple phytoplankton zooplankton system

Brajendra K. Singh[a], Joydev Chattopadhyay[b], Somdatta Sinha[a,*]

[a]*Centre for Cellular and Molecular Biology, Uppal Road, Hyderabad, A.P. 500 007, India*
[b]*Biomathematics Group, Agricultural Sciences Unit, Indian Statistical Institute, 203, B.T. Road, Kolkata 700 108, India*

Received 29 August 2003; received in revised form 2 June 2004; accepted 14 June 2004
Available online 12 August 2004

Abstract

Many planktonic species show spectacular bursts (''blooms'') in population density. Though viral infections are known to cause behavioural and other changes in phytoplankton and other aquatic species, yet their role in regulating the phytoplankton population is still far from being understood. To study the role of viral diseases in the planktonic species, we model the phytoplankton–zooplankton system as a prey–predator system. Here the prey (phytoplankton) species is infected with a viral disease that divides the prey population into susceptible and infected classes, with the infected prey being more vulnerable to predation by the predator (zooplankton). The dynamical behaviour of the system is investigated from the point of view of stability and persistence both analytically and numerically. The model shows that infection can be sustained only above a threshold of force of infection, and, there exists a range in the infection rate where this system shows ''bloom''-like stable limit cycle oscillations. The time series of natural ''blooms'' with different types of irregular oscillations can arise in this model simply from a biologically realistic feature, i.e., by the random variation of the epidemiological parameter (rate of infection) in the infected prey population. The difference in mean strength of infection alone can lead to the different types of patterns observed in natural planktonic blooms.

Keywords: Phytoplankton–zooplankton; Virus infection; Phytoplankton blooms; Lotka–Volterra model; Prey–predator interactions; Limit cycle oscillations

1. Introduction

Transmissible diseases are known to induce major behavioural changes in aquatic species. However, little attention has been paid to model such situations to predict useful applications in both dynamics and control. There are many examples of parasites modifying the behaviour of the infected individuals of the host population. This may happen by reducing stamina, disorientation and altering responses (Holmes and Bethel, 1972). Lafferty and Morris (1996) observed that kill fish (*Fundulus parvipinnes*) tends to come closer to the surface of the sea on contracting a disease, which makes them more vulnerable to predation by birds. Arme and Owen (1967) and Williams (1967) observed the same behaviour in sticklebacks (*Gasterosteus awleatus L.*) infected by plerocarcoids (*Schistocephalus solidus*). Viral infection can also cause cell lysis in phytoplankton. Using electron microscopy, Suttle et al. (1990) showed that viral disease can infect bacteria and phytoplankton in coastal water. Virus like particles have been described in many eukaryotic algae (van Etten et al., 1991; Reisser, 1993), cyanobacteria (Suttle et al., 1993) and natural phytoplankton communities (Peduzzi and Weinbauer, 1993).

Many planktonic species show spectacular bursts (''blooms'') in population density. The periodic nature of blooms, in the sense of the rapid onset and disappearance of oscillations, is one of the main characteristics in plankton ecosystem. In a broad sense

*Corresponding author. Tel.: +91-40-27-192588; fax: +91-40-27-160591.
E-mail address: sinha@ccmb.res.in (S. Sinha).

0022-5193/$ - see front matter © 2004 Elsevier Ltd. All rights reserved.
doi:10.1016/j.jtbi.2004.06.010

planktonic blooms may be defined into two types, "spring blooms" and "red tides". Spring blooms occur seasonally due to changes in temperature or nutrient availability. Red tides are localized outbreaks associated with water temperature, greater stability of the water column as well as higher growth rates (Truscott and Brindley, 1994). Different criteria has been used in the literature to define and classify "bloom" (Agusti et al., 1987; Smayda, 1997a, b). Biomass is the common criterion for non-toxic species, whereas for harmful species mere presence or measurable toxin levels are responsible for the bloom dynamics. Field and experimental evidences reveal different modes and mechanisms by which harmful species can cause mortality and thereby induce the observed dynamics. Viruses have been held responsible for the collapse of *Emiliania huxleyi* blooms in mesocosms (Bratbak et al., 1995) and in the North Sea (Brussaard et al., 1996) and have been shown to induce lysis of Chrysochromulina (Suttle and Chan, 1993). Because viruses are sometimes strain-specific, they can increase genetic diversity (Nagasaki and Yamaguchi, 1997). Nevertheless, despite the increasing number of reports, the role of viral infection in the phytoplankton population is still far from understood.

Being a primary producer, phytoplankton bloom dynamics is known to affect other species significantly in the upper food chain (Platt et al., 2003). Yet, few theoretical studies have been carried out for such eco-epidemiological systems, where the effect of viral infection on plankton ecology has been explored (Hadeler and Freedman, 1989; Freedman, 1990; Beltrami and Carroll, 1994; Venturino, 1995; Chattopadhyay and Arino, 1999; Chattopadhyay et al., 1999; Chattopadhyay and Pal, 2002; Xiao and Chen, 2001). The present paper aims to study the role of infection on the induction of "bloom" like phenomena in a phytoplankton–zooplankton system and attempts to describe the natural "bloom" patterns with variations in the epidemiological parameter.

1.1. Previous theoretical results and our motivation

Beltrami and Carroll (1994) proposed a model to discuss the role of viral disease in recurrent phytoplankton blooms. They analysed a prey–predator system in which some of the susceptible phytoplankton cells were infected by viral contamination and formed a new group (infected). Based primarily on numerical simulations and meagre theoretical analysis, they concluded that a minute amount of infectious agent can de-stabilize the otherwise stable trophic configuration between a phytoplankton species and its grazer. Standard epidemiological models (Anderson and May, 1991) indicate that generally a minimum threshold of infection is observed below which the infected population does not persist and hence the disease does not spread. The condition for Hopf-bifurcation was also given in their paper, which is satisfied when the contact rate equals the rate of cell lysis. From ecological view point this is not plausible. To model the natural bloom pattern which looks erratic, they assumed temperature-cycle regulated growth rate of the susceptible prey population. It is not surprising that they get chaotic oscillations in such a periodically forced system. They compared their results to the actual data by a nonlinear forecasting technique. The other authors have generally ignored the behaviour of limit cycle oscillations.

In this paper we propose a prey–predator model for the phytoplankton–zooplankton system with the assumption that the viral disease is spreading only among the prey species, and, though the predator feeds on both the susceptible and infected prey, the infected prey is more vulnerable to predation as is seen in nature (see references quoted earlier). The dynamical behaviour of the system is investigated from the point of view of stability and persistence. The model shows that infection can be sustained only above a threshold of force of infection. Also, the system is locally asymptotically stable in some region of the parametric space and exhibits periodic oscillations in some other region. The stability of the limit cycles arising from Hopf bifurcation is analysed using the centre manifold theorem. Numerical simulations substantiate the analytical results, and show the variation in the dynamic behaviour of the system with increasing rate of infection. The viral disease not only induces burst-like periodic oscillations in the phytoplankton–zooplankton populations, it also allows persistence and stability in the system.

Assuming that the infected prey cells may vary in their ability to cause infection in susceptible preys, we have shown that such a realistic demographic feature is sufficient to give rise to the patterns of irregularity observed in natural planktonic blooms (Tont, 1976; Uhlig and Sahling, 1992). We show that the difference in mean strength of infection alone can lead to the different types of the bloom patterns observed in host phytoplanktons.

2. The model

(A1) We consider a two species ecological system with phytoplankton (prey) and its grazer, the zooplankton (predator), whose total population densities are denoted by N and P, respectively, in units of number of cells/l. The phytoplankton is assumed to be susceptible to a viral disease, and in the presence of viruses, the total phytoplankton population is divided into two classes—susceptible prey (S) and infected prey (I).

(A2) We assume that the susceptible prey species reproduces following the law of logistic growth with

carrying capacity M, and intrinsic birth rate a

$$\frac{dS}{dt} = aS\left(1 - \frac{N}{M}\right). \quad (1)$$

Experiments on dinoflagellate *Noctiluca scintillans* (milliaris) have suggested that in the German Bight disease the organisms become damaged and they do not feed anymore or reproduce (Uhlig and Sahling, 1992). The model of Hamilton et al. (1990) showed that infected individuals fail to contribute in the reproduction process due to their inability to compete for resources. Though the infected individuals are handicapped with respect to resource competition, they can still affect the growth dynamics of the susceptibles indirectly—for example, by shading. Based on the above, we assume that the infected prey may contribute to the carrying capacity. Therefore, the term N/M in Eq. (1) becomes $(S+I)/M$. Eq. (1) then takes the form

$$\frac{dS}{dt} = aS - bS(S+I), \quad (2)$$

where, $b = a/M$.

(A3) We assume that the disease spreads only among the prey, and the predator population is not infected due to predation of infected prey. Also, as mentioned earlier, the infected prey is more vulnerable to predation than the susceptible prey as has been observed in several natural systems.

(A4) A susceptible prey S becomes infected under the attack of many viruses. The contact process is admittedly debatable. Some researchers argue that a proportional mixing rate is more appropriate than that of simple mass action. But the data of Greenwood experiment suggests that there is no change of qualitative properties upon the contact process whether it follows the law of mass action or proportional mixing rate (De Jong et al., 1994).

Considering the above we can write the following equations describing the time evolution of the phytoplankton–zooplankton system:

$$\begin{aligned}\frac{dS}{dt} &= aS\left(1 - \frac{b}{a}(S+I)\right) - cSP - \lambda SI,\\ \frac{dI}{dt} &= I(\lambda S - kP - h),\\ \frac{dP}{dt} &= P(-d + eS + k_1 I). \end{aligned} \quad (3)$$

Here S and I are the concentrations of the susceptible and the infected prey phytoplanktons, respectively; and P is the concentration of the predator zooplankton, at time t. The parameters a denotes the intrinsic rate of increase of susceptible prey; b relates to the carrying capacity or crowding effects of the prey; c is the capture rate of the susceptible prey by the predator; d denotes the death rate of predators in the absence of prey; e is the growth rate of predators due to predation of susceptible prey; k denotes the rate of capturing of infected prey by the predators; h is the death rate of infected phytoplankton; λ is the force of infection between susceptible and infected prey populations; and k_1 is the growth rate of predator due to predation of infected phytoplankton ($k_1 \leqslant k$).

Since the infected prey is prone to higher predation when compared to the susceptible prey (see (A3)), k is considered to be greater than c.

2.1. Equilibria

System (3) possesses the following equilibria:

$$E_0(0,0,0), \quad E_1\left(\frac{a}{b},0,0\right), \quad E_2\left(\frac{d}{e},0,\frac{ae-bd}{ec}\right),$$
$$E_3\left(\frac{h}{\lambda},\frac{a\lambda - bh}{\lambda(\lambda+b)},0\right)$$

and the positive interior equilibrium $E^*(S^*, I^*, P^*)$, where

$$S^* = \frac{-\lambda kd + akk_1 + chk_1 - bdk}{A_2}, \quad (4)$$

$$I^* = \frac{-aek + c\lambda d + bkd - che}{A_2}, \quad (5)$$

$$P^* = \frac{-\lambda^2 d + a\lambda k_1 + \lambda eh - bk_1 h - bd\lambda + bhe}{A_2}, \quad (6)$$

where

$$A_2 = c\lambda k_1 - \lambda ke + bkk_1 - bke. \quad (7)$$

Along with the assumption $k > c$, for positive and non-zero A_2 one gets the additional condition $k_1 > e$. This means that the growth rate of the predator due to predation of the infected prey (k_1) is higher than that of the susceptible prey (e).

The positivity and existence of the interior equilibrium (E^*) lead to conditions based on which a range of the force of infection (minimum and maximum λ) can be obtained from Eqs. (4)–(6). Eqs. (4) and (5) give two values of λ, and Eq. (6) also gives two positive roots for λ. Calculation shows that the range of λ, between which the E^* exists, is given by

$$\lambda_{min} = \left(\frac{1}{c}\right)\left[\frac{ake + che}{d} - bk\right],$$
$$\lambda_{max} = \frac{1}{2d}[(eh + ak_1 - bd) + \sqrt{(eh + ak_1 - bd)^2 - 4bhd(k_1 - e)}]. \quad (8)$$

3. Local asymptotic stability (LAS) analysis

Here we summarize the results of the local stability of system (3) around each of the equilibria. The details are given in Appendix A and B.

The LAS of the equilibria obtained in Section 2 are

(i) E_0 is unstable.
(ii) LAS of E_1 implies the non-existence of E_2 and E_3.
(iii) Existence of a positive interior equilibrium (E^*) implies that E_2 is unstable.
(iv) Existence of a positive E^* implies that E_3 is unstable.
(v) The dynamical behaviour of system (3) around the positive E^* depends on the parameter values. System (3) is locally asymptotically stable in some region of parameter space, and shows limit cycle oscillations at some other regions. Eq. (8) gives the interval $[\lambda_{min}, \lambda_{max}]$ for the force of infection, λ, within which E^* exists. Choosing λ, as a bifurcation parameter, it can be shown that
  (v.a) For $\lambda < \lambda_{min}$, E^* does not exist as the infection does not persist; and, for $\lambda > \lambda_{max}$ the infection rate is too high for E^* to exist.
  (v.b) The interval $[\lambda_{min}, \lambda_{max}]$ contains a critical value λ_{cr}, where a supercritical Hopf bifurcation occurs. For λ between λ_{min} and λ_{cr}, the interior equilibrium is asymptotically stable. For λ between λ_{cr} and λ_{max}, a limit cycle exists.

4. Numerical study of the system behaviour

The dynamics of system (3) around the positive interior steady state has been numerically simulated for a range of parameter values. The parameters values used are taken from literature (Beltrami and Carroll, 1994; Chattopadhyay and Pal, 2002). They are

$$b = 0.006, \quad c = 0.06, \quad d = 0.4, \quad e = 0.01, \quad h = 0.5$$
$$k = 0.1, \quad k_1 = 0.08.$$

These also satisfy the conditions $k > c$ and $k_1 > e$.

The growth rate (a) of the susceptible prey S and the force of infection (λ) are the two parameters that directly influence the population density of the preys. Thus, we have studied the dynamics of the system for a wide variation in a ($0 < a < 12$) and λ ($0 < \lambda < 3$). The carrying capacity (M) has also been studied by doubling its value to show that the results are valid for fairly different environments of the prey.

4.1. Dynamics of the system for increasing rate of infection (λ)

The dynamics of the susceptible prey population (for $a = 5$), around E^*, for increasing λ is shown in the bifurcation plot in Fig. 1. The plot shows that the effect of increasing λ is two-fold.

(a) The infected phytoplankton population does not persist below a minimum strength (threshold) of infection (λ_{min}), and hence, the disease does not spread in the prey population. For $\lambda > \lambda_{min}$, there is a small range of λ (shown by thick line) where both the susceptible and infected phytoplankton species co-exist at equilibrium with their predator zooplankton.

(b) Increasing λ further induces instability in the system through a supercritical Hopf bifurcation at $\lambda = 0.20527$. (This corresponds very well to the values obtained from the analysis given in the Appendix.) Limit cycle oscillations with fast increasing amplitude are observed which attains a maximum at $\lambda \approx 0.36$. Thereafter the amplitude of oscillation decreases with increasing λ, and, finally reduces to zero as λ approaches a high value (λ_{max}) beyond which the fixed point E^* does not exist. Thus, there exists a range of force of infection within which both the prey and predator populations co-exist, and can exhibit large amplitude oscillations.

The figure also shows that the response of the phytoplankton population to increasing force of infection is highly nonlinear and, a small increase in infectivity at lower λ induces a larger effect when compared to the effect of a comparable increase at higher values of λ.

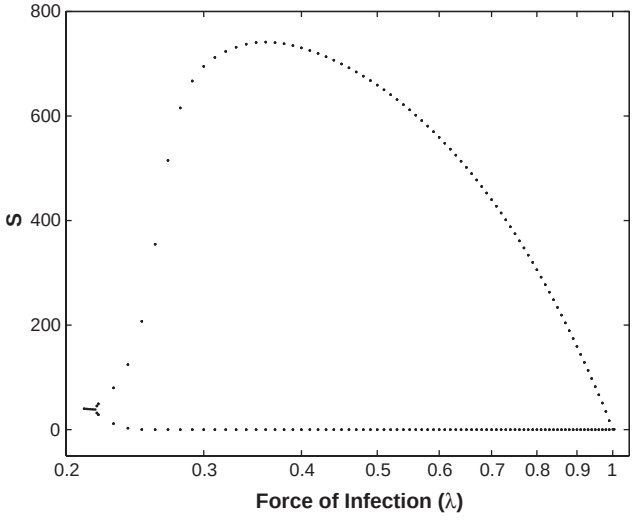

Fig. 1. Bifurcation diagram of S with increasing force of infection, λ, for growth rate $a = 5$. X-axis is plotted in logarithmic scale to highlight the short range of small values of λ where the dynamics is in equilibrium.

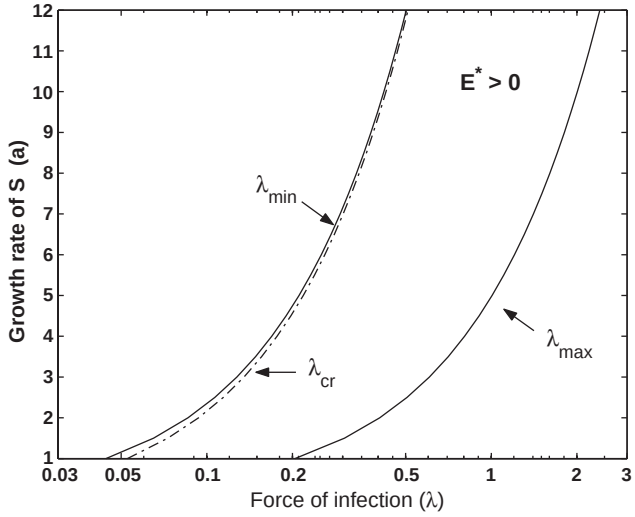

Fig. 2. Stability plot in the $(\lambda - a)$ parameter space. X-axis is in logarithmic scale to delineate the small difference between λ_{min} and λ_{cr}.

4.2. Population stability in $(\lambda - a)$ parameter space

Fig. 2 shows the stability of the system (Eq. (3)), obtained through linear stability analysis, for variation in both the force of infection (λ) and the intrinsic growth rate (a). Here λ is plotted in logarithmic scale in the X-axis, and λ_{min} and λ_{max} are obtained from Eq. (8). The curves in Fig. 2 show the following results:

(a) Both λ_{min} and λ_{max} are increasing functions of the growth rate a of the susceptible prey. The distance between the two curves is finite for all non-zero, positive and realistic parameter values (i.e., $b, k > 0$ and $c < \infty$), and increases with increasing a. Thus, this system of phytoplankton (susceptible and infected) and their predator zooplankton co-exist for a larger range of values of the force of infection λ for prey species with higher growth rates. This result is valid for a wide range of values of the other parameters (e.g., the carrying capacity of the prey species (b), attack and utilization rates of preys (c and e), and the death rate (d) of the predators).

The infected prey $I > 0$ only for $\lambda > \lambda_{min}$, indicating that there is a minimum threshold of the force of infection for all a, below which the infected population does not persist and hence the disease does not spread. This threshold increases with increasing a. It may be noted that this result is also consistent with the standard epidemiological models such as, the SEIR models (Anderson and May, 1991).

(b) There exists a critical value of the force of infection, (λ_{cr}), between the λ_{min} and λ_{max}, where the dynamics of the interior steady state E^* goes through a supercritical Hopf bifurcation (see Appendix A). Thus, the system shows equilibrium dynamics for $\lambda_{min} < \lambda < \lambda_{cr}$, and periodic dynamics for $\lambda_{cr} < \lambda < \lambda_{max}$. The λ_{cr} line also increases with a. The equilibrium dynamics in this system is observed for a small range of force of infection, and this range becomes narrower at higher growth rates. Thus the predominant dynamics exhibited by this system is oscillatory and hence, "bloom" is an inherent dynamic property of this system.

4.3. Temporal evolution of the populations

The bifurcation diagram in Fig. 1 gives an indication of the large variation in the amplitude of oscillations in S at different values of λ. In Fig. 3 we show the temporal properties of S, i.e., amplitude and time period, for different values of force of infection λ for $a = 5$. Fig. 3(a) shows the time series where the amplitude of oscillations is higher for medium value of λ (dot-dashed line for $\lambda = 0.4$), compared to both low (continuous line for $\lambda = 0.23$) and high (dotted line for $\lambda = 0.7$) values. The maximum population size of S changes in a nonlinear fashion with increasing force of infection. A

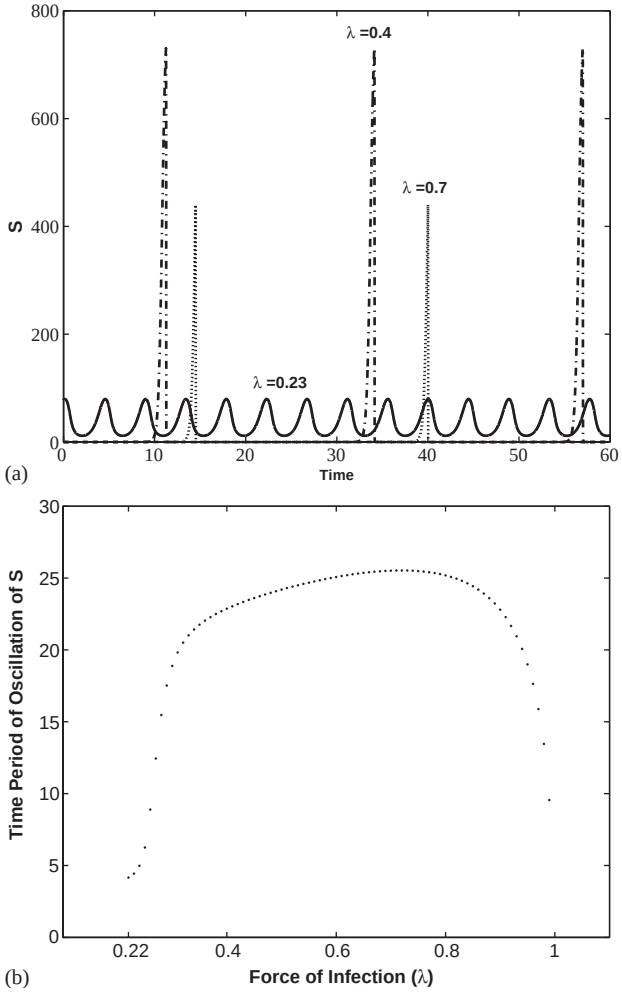

Fig. 3. (a) Time series of S at three different values of force of infection λ (0.23, 0.4 and 0.7) for $a = 5$. (b) Time period of oscillations of S for different values of λ for $a = 5$.

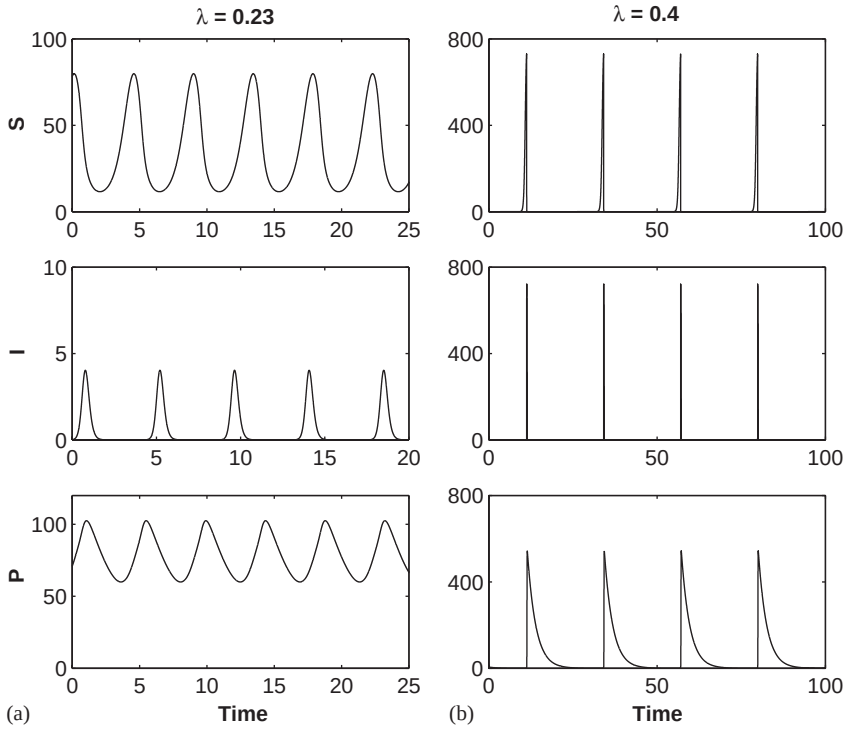

Fig. 4. Time evolution of S, I and P for $a = 5$ at (a) low force of infection, $\lambda = 0.23$, and (b) medium force of infection, $\lambda = 0.4$.

small change in λ at lower values leads to faster increase in the maximum population size, whereas, it decreases much slowly at higher values of λ. Also, at medium and higher values of λ, the nature of the oscillations of the phytoplankton population appears as sudden bursts (''bloom-like'') separated by low population density for long stretches of time.

The force of infection λ also affects the frequency of the periodic bursts in the phytoplankton population in a nonlinear manner. Fig. 3(b) shows the variation in the time period of oscillation in S with increasing λ. It is clear that the frequency of oscillation is quite high at small and large values of λ, but it maintains a fairly low value for an extended range of force of infection. The time period changes maximally only by 7 units in the range of λ between 0.3 and 0.95, whereas, a large change of 14 units is observed from $\lambda = 0.23$ to 0.3. Thus, within the range of the force of infection where the prey and predator populations co-exist, the system primarily shows burst-like oscillations with time period about 23 units.

Along with S, λ regulates the abundance of the infected phytoplankton and the predator zooplankton population. Fig. 4 depicts the time series showing the effect of increased λ ($\lambda = 0.23$ and 0.4) on the abundance of S, I and P for $a = 5$. At low values of λ (Fig. 4(a)), the infected species I is present in very low amounts. In this case the predator primarily predates on the susceptible prey. The time period and amplitude of oscillations of S and P are also small, and the population sizes show a regular increase and decrease throughout the cycles. In contrast to the above, even though the growth rate of prey is the same as in Fig. 4(a), Fig. 4(b) shows that the population of I grows quite rapidly, and both the preys and predator reach high population size on increasing λ. The plankton population oscillations are burst-like and occur with slower frequency. The population of the infected prey peaks almost immediately after the susceptible prey peaks, and the predator population rises very rapidly with the growth of the prey species inducing a sharp decline in population of the preys. The predator population then decreases continuously in response to low prey population. This trend continues for an extended range of λ values.

4.4. Modelling the natural ''bloom'' pattern

The phytoplankton ''blooms'' in nature (see Figs. 5(a) and (b)) have irregular amplitude and time period. The time series shown in Fig. 5(a) for the species *Noctiluca scintillans* in German Bight shows clear isolated bursts occurring fairly regularly (Uhlig and Sahling, 1992). The time series in Fig. 5(b) of the diatom species (Tont, 1976), on the other hand, shows clusters of bursts with unequal amplitudes and variable time period. The population density is much higher for the species in Fig. 5(b) in comparison to the one in Fig. 5(a). The ''noisiness'' in the amplitude of the phytoplankton

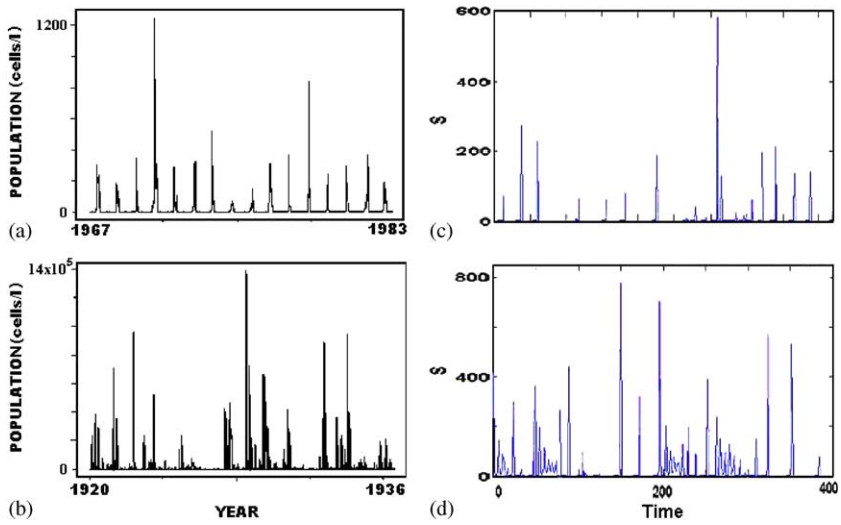

Fig. 5. Phytoplankton "bloom" patterns: (a) *Noctiluca scintillans* in the German Bight from 1967 to 1983, and (b) Diatom abundance from 1920 to 1936. Simulated density of S for noisy λ with mean at (c) 0.95, and (d) 0.4.

blooms as seen in real data has been modelled by Beltrami and Carroll (1994) using a forcing term (temperature cycle-regulated growth rate of the prey), which leads to chaotic oscillations. It is commonly understood in theory that chaos can be achieved through forcing an oscillating system. But advancing such a reason for the irregularity in oscillation amplitude requires some (experimental or empirical) proof showing regular oscillations under constant temperature.

Based on our results, we take a different approach, and show that these real time series can arise from our model under a simple but realistic assumption. From Figs. 3 and 4 it is obvious that a range of medium infectivity is responsible for periodic blooms in the phytoplankton–zooplankton system, as very low and very high values of λ lead to severe reduction in the prey and predator population sizes, and thus, may not be evolutionarily selected. In a population of phytoplankton cells, the force of infection (effectively decided by the number of viruses in each infected cell) can vary due to intrinsic noise in cellular processes (Bergh et al., 1989; McAdams and Arkin, 1999) leading to variation in the strength of infection around some mean value. Given that the maximum of the amplitude depends quite sensitively on λ (see Figs. 1 and 2), small variation in λ can induce large changes in bloom amplitude. The time-period does not change appreciably for medium values of λ (between 0.4 and 0.95), though it is quite small for both low and high values of infectivity (see Fig. 3(b)). Thus, depending on the mean value of the infectivity of the virus, the phytoplankton population may exhibit different temporal patterns of "bloom" with irregular amplitude and constant or variable time period.

Figs. 5(c) and (d) show simulations from our model (Eq. (3)) where λ is varied randomly from an exponential distribution with mean λ as 0.95 for Fig. 5(c) and 0.4 for Fig. 5(d). We use exponential distribution under the assumption that infection is a Poisson process (Edelstein-Keshet, 1988), and that infected cells with high values of λ will be less likely to occur in a population. Fig. 5(c) shows single bursts of small and varying amplitude, and Fig. 5(d) shows clusters of small amplitude bursts with large occasional peaks and variable time period. It is clear from these figures that different types of oscillations can arise in the same system depending on the average strength of the viral infection (or, host immunity). Lower mean λ results in clustered oscillations with high peak, whereas larger mean λ shows more periodic but unequal amplitude single bursts. Our results thus show that the natural phytoplankton blooms can arise from demographic noise in λ, and that the nature of these blooms may change depending on the host (phytoplankton) and virus species.

5. Discussion

Periodic nature of blooms i.e., the rapid onset and disappearance of oscillations under supposedly favourable environmental condition, is one of the main characteristics in plankton ecosystem. Reports of high abundance of viruses in aquatic environments are known for quite some time, and their role in regulating the phytoplankton community structure and primary productivity in oceans have been implicated (Bergh et al., 1989, Suttle et al., 1990). That the recurrent "blooms" in different species of the primary producers

may be due to life history changes induced by viral infection is considered in this paper. We have used a three variable Lotka–Volterra (LV) like system of equations to model the phenomena and shown that limit cycle oscillations, that is considered to underlie the formation of bloom, can occur for a large region in the parameter space.

Needless to say that viral infection is not the only mechanism that can give rise to limit cycle oscillations in a prey–predator system. There is a large body of literature where the phytoplankton blooms have been modelled using realistic modifications in the classical prey–predator model by incorporating the nonlinear functional responses of the phytoplankton–zooplankton system or using environmental forcing. For example, limit cycle oscillations can be found in a simple LV system if the functional response of the predator population is not constant but density dependent with different nonlinear forms (Rosenzweig and MacArthur, 1963; Murray, 1989; Steele and Henderson, 1993). Conditions for phytoplankton bloom development have been extensively investigated in well-mixed aquatic systems with homogeneous phytoplankton density using integro-differential equations (Platt et al., 1991; Weissing and Huisman, 1994). The bloom dynamics under incomplete mixing of phytoplankton, including spatial patchiness, nutrient upwelling, species diversity, light gradients and critical turbulence as is seen in oceans, have also been studied (Edwards and Brindley, 1996; Mathews and Brindley, 1996; Pitchford and Brindley, 1998; Huisman et al., 1999; Ebert et al., 2001). External forcing can induce oscillations in a simple prey–predator system (Inoue and Kamifukumoto, 1984). Ecological communities are generally embeded in periodically varying environments. It has been shown (Rinaldi et al., 1993) that such periodic external forcing may lead a classical prey–predator system into Hopf bifurcation, period doubling, and chaos.

In this paper we proposed and analysed, both analytically and numerically, a simple phytoplankton (prey)–zooplankton (predator) system in which some members of the phytoplankton population are infected by a transmissible disease, thereby, forming a new group (the infected prey), which is more vulnerable to predation. This disease-regulated differential mortality of the prey population leads to several changes in the dynamics of this system.

When there is no infection affecting the prey population, i.e., $I = 0$, the three variable system considered in Eq. (3) reduces to the simple two variable prey–predator system with prey growing according to the logistic growth law. Local stability analysis of the non-trivial steady state $(S^*, P^* > 0)$ shows that this system is always stable for growth rate $a \geqslant 1$. (Note that the only possibility for oscillations to occur is when $b = 0$, or $d = 0$, or $e = \infty$. Since the last two conditions are not realistic, the condition $b = 0$ points to an environment where the carrying capacity of the prey species is infinite. With this condition it then reduces to the two variable classical Lotka–Volterra type prey–predator system which shows structurally unstable periodic dynamics.)

We have obtained conditions for small amplitude periodic solutions bifurcating from a positive interior equilibrium by applying both mathematical and numerical techniques. The stability as well as the direction of bifurcation is obtained by applying the algorithm due to Hassard et al. (1981) that depends on the centre manifold theorem. We have then used numerical simulation for a large range of parameters to study the dynamics and persistence under increasing force of infection. The role of disease in the prey population has two major aspects. First, there is a minimum and a maximum force of infection below and above which the three species do not co-exist. Thus the disease does not spread for $\lambda < \lambda_{min}$. This kind of a threshold response is known in epidemiology (Kermack and McKendrick, 1927), and is different from the earlier result (Beltrami and Carroll, 1994) where even a minute amount of infectious agent is shown to destabilize the otherwise stable trophic configuration between a phytoplankton species and its grazer.

Secondly, the dynamics of the coexisting populations show stable dynamics for a small range of force of infection. Increasing the force of infection destabilizes the system through a supercritical Hopf bifurcation and the populations show large amplitude "bloom" type of oscillatory dynamics, as seen in the phytoplankton populations in nature. Within the range of co-existence, the predominant dynamics exhibited by this system is oscillatory. Our results show that infection increases the population burst in the phytoplankton species quite dramatically, although the time period remains fairly uniform for a large range of λ. Thus the disease not only induces and increases the oscillatory tendency in the population, it also increases the maximum population size of both the preys and the predator.

Finally we have shown that realistic assumption of variability of infectivity among the cells can give rise to phytoplankton blooms of the kind seen in nature. Given the increasing reports on viral infection of phytoplanktonic communities, our theoretical study indicates an important role of infection in the phytoplankton–zooplankton system in inducing the blooms. These results, therefore, urge that more attention be given to the epidemiological aspects of these ecological systems.

Acknowledgements

This paper has improved considerably, both in presentation and scientific content, by the critical

comments made by the anonymous reviewers. The authors are thankful to them. Thanks are also due to Dr. C. Suguna for computational help, and Drs. A. Mukhopadhyay and R. Sarkar for critical reading of the paper.

Appendix A. Local asymptotic stability (LAS) analysis

The local stability of system (3) around each of the equilibria is obtained by computing the variational matrix corresponding to each equilibrium.

The variational matrix around $E^*(S^*, I^*, P^*)$ is

$$V(S^*, I^*, P^*) = \begin{bmatrix} a - 2bS^* - cP^* - \lambda I^* - bI^* & -(\lambda + b)S^* & -cS^* \\ \lambda I^* & \lambda S^* - kP^* - h & -kI^* \\ eP^* & k_1 P^* & -d + eS^* + k_1 I^* \end{bmatrix},$$

The variational matrix for E_0 is

$$V_0 = \begin{bmatrix} a & 0 & 0 \\ 0 & -h & 0 \\ 0 & 0 & -d \end{bmatrix}.$$

The eigenvalues are $\mu_1 = a > 0$, $\mu_2 = -h < 0, \mu_3 = -d < 0$, which shows that E_0 is unstable.

The variational matrix for E_1 is

$$V_1 = \begin{bmatrix} -a & -\frac{\lambda a}{b} & -\frac{ca}{b} \\ 0 & \frac{\lambda a}{b} - h & 0 \\ 0 & 0 & -d + \frac{ea}{b} \end{bmatrix}.$$

The eigenvalues are $\mu_1 = -a < 0$, $\mu_2 = (\lambda a/b) - h$, $\mu_3 = -d + ea/b$. From the above it is clear that LAS of E_1 implies the non-existence of E_2 and E_3.

The variational matrix for E_2 is

$$V_2 = \begin{bmatrix} \frac{-bd}{e} & \frac{-\lambda d}{e} & \frac{-dc}{e} \\ 0 & \frac{\lambda dc - k(ae-bd) - hec}{ec} & 0 \\ \frac{(ae-bd)}{c} & \frac{k_1(ae-bd)}{ec} & 0 \end{bmatrix}.$$

The characteristic equation for E_2 is

$$\left[\frac{\lambda dc - k(ae - bd) - hec}{ec} - \mu\right]\left[\left(\frac{bd}{e} + \mu\right)\mu + \frac{d(ae - bd)}{e}\right] = 0.$$

The eigenvalues are

$$\mu_1 = \frac{\lambda dc - k(ae - bd) - hec}{ec}$$

and the other two roots are given by

$$\mu^2 + \mu K_1 + K_2 = 0,$$

where $K_1 = bd/e > 0$, $K_2 = d(ae - bd)/e > 0$.

It is clear from (5) that $\lambda dc - k(ae - bd) - hec > 0$, so $\mu_1 > 0$ and hence the existence of a positive interior equilibrium implies that E_2 is unstable. Note that non-existence of a positive interior equilibrium ensures that E_2 is stable.

The variational matrix for E_3 is

$$V_3 = \begin{bmatrix} \frac{-bh}{\lambda} & -h & \frac{-ch}{\lambda} \\ \frac{a\lambda - bh}{\lambda} & 0 & \frac{-k(a\lambda - bh)}{\lambda^2} \\ 0 & 0 & \frac{-d\lambda^2 + eh\lambda + k_1(a\lambda - bh)}{\lambda^2} \end{bmatrix}.$$

The characteristic equation for E_3 is

$$V_3 = \begin{bmatrix} \frac{-bh}{\lambda} & -\frac{(\lambda+b)h}{\lambda} & \frac{-ch}{\lambda} \\ \frac{a\lambda - bh}{b+\lambda} & 0 & \frac{-k(a\lambda - bh)}{\lambda(b+\lambda)} \\ 0 & 0 & \frac{-d\lambda(b+\lambda) + eh(b+\lambda) + k_1(a\lambda - bh)}{\lambda(b+\lambda)} \end{bmatrix}.$$

The characteristic equation for E_3 is

$$\left[\frac{-d\lambda(b + \lambda) + eh(b + \lambda) + k_1(a\lambda - bh)}{\lambda(b + \lambda)} - \mu\right] \times \left[\mu\left(\frac{bh}{\lambda} + \mu\right) + \frac{(\lambda + b)h}{\lambda}\left(\frac{a\lambda - bh}{b + \lambda}\right)\right] = 0$$

and hence the eigenvalues are

$$\mu_1 = \frac{-d\lambda(b + \lambda) + eh(b + \lambda) + k_1(a\lambda - bh)}{\lambda(b + \lambda)} > 0$$

(for $P^* > 0$)

and the other two roots are given by

$$\mu^2 + \mu l + l' = 0$$

where,

$$l = \frac{bh}{\lambda} > 0, \quad l' = \frac{(\lambda + b)h}{\lambda}\left(\frac{a\lambda - bh}{b + \lambda}\right) > 0.$$

It is clear that existence of a positive interior equilibrium implies that $\mu_1 > 0$ and hence E_3 is unstable.

Now, we shall study the dynamical behaviour of system (3) around the positive interior equilibrium (E^*). We choose λ as the bifurcation parameter. The interval $[\lambda_{min}, \lambda_{max}]$ within which E^* exists is given by Eq. (7). Here we show that in the interval $[\lambda_{min}, \lambda_{max}]$, there exists a critical value λ_{cr}, where a supercritical Hopf bifurcation occurs. Thus under the conditions $k > c$ and $k_1 > e$, and in the interval $[\lambda_{min}, \lambda_{max}]$, the interior equilibrium is

asymptotically stable between λ_{min} and λ_{cr}. For λ between λ_{cr} and λ_{max}, a limit cycle exists.

To find λ_{cr}, we use the variational matrix for E^*

$$V_* = \begin{bmatrix} -bS^* & -(\lambda+b)S^* & -cS^* \\ \lambda I^* & 0 & -kI^* \\ eP^* & k_1P^* & 0 \end{bmatrix}. \quad (A.1)$$

The characteristic equation is given by

$$\mu_*^3 + d_1\mu_*^2 + d_2\mu_* + d_3 = 0 \quad (A.2)$$

where

$$d_1 = bS^*,$$
$$d_2 = kk_1I^*P^* + \lambda^2 I^*S^* + ceS^*P^* + \lambda bS^*I^*,$$
$$d_3 = kk_1bS^*I^*P^* - ke\lambda S^*I^*P^* + c\lambda k_1S^*I^*P^* - kebS^*I^*P^*. \quad (A.3)$$

By the Routh–Hurwitz criterion, a set of necessary and sufficient conditions for all the roots of (A.1) to have negative real part is $d_1>0$, $d_2>0$ (which are obvious) and $d_1d_2>d_3$ (a sufficient condition for this is $ke=ck_1$). Also, $d_3>0$ if $k_1>e$ and $ke=ck_1$. Thus system (3) is locally stable around the positive interior equilibrium (E^*) when $ke=ck_1$ along with $k_1>e$.

Necessary and sufficient conditions for Hopf bifurcation to occur are that there exists a $\lambda=\lambda_{cr}$, such that

(i) $d_i(\lambda_{cr})>0, \quad i=1,2,3,$

(ii) $g(\lambda_{cr}) \equiv d_1(\lambda_{cr})d_2(\lambda_{cr}) - d_3(\lambda_{cr}) = 0$

and

(iii) $Re\left[\frac{d\mu_j}{d\lambda}\right]_{\lambda=\lambda_{cr}} \neq 0, \quad j=1,2,3.$

The condition $d_1d_2-d_3=0$ is given by

$$H \equiv bceP^*S^{*^2} + b\lambda^2 I^*S^{*^2} + ke\lambda P^*S^*I^* - c\lambda k_1S^*I^*P^* = 0. \quad (A.4)$$

Since $d_2>0$ at $\lambda=\lambda_{cr}$, there is an interval containing λ_{cr}, say $(\lambda_{cr}-\varepsilon, \lambda_{cr}+\varepsilon)$ for some $\varepsilon>0$ for which $\lambda_{cr}-\varepsilon>0$ such that $d_2>0$ for $\lambda\in(\lambda_{cr}-\varepsilon,\lambda_{cr}+\varepsilon)$. Thus for $\lambda\in(\lambda_{cr}-\varepsilon,\lambda_{cr}+\varepsilon)$, the characteristic Eq. (A.1) cannot have real positive roots. For $\lambda=\lambda_{cr}$, we have

$$(\mu^2+d_2)(\mu+d_1)=0, \quad (A.5)$$

which has three roots $\mu_1=+i\sqrt{d_2}, \mu_2=-i\sqrt{d_2}, \mu_3=-d_1$.

For $\lambda\in(\lambda_{cr}-\varepsilon,\lambda_{cr}+\varepsilon)$, the roots are, in general, of the form

$$\mu_1(\lambda)=\beta_1(\lambda)+i\beta_2(\lambda),$$
$$\mu_2(\lambda)=\beta_1(\lambda)-i\beta_2(\lambda),$$
$$\mu_3(\lambda)=-d_1(\lambda).$$

Now, we shall verify the transversality condition

$$Re\left[\frac{d\mu_j}{d\lambda}\right]_{\lambda=\lambda_{cr}} \neq 0, \quad j=1,2. \quad (A.6)$$

Substituting $\mu_j(\lambda)=\beta_1(\lambda)+i\beta_2(\lambda)$ into (A.5) and calculating the derivative, we have

$$K(\lambda)\beta_1'(\lambda) - L(\lambda)\beta_2'(\lambda) + M(\lambda) = 0,$$
$$L(\lambda)\beta_1'(\lambda) + K(\lambda)\beta_2'(\lambda) + N(\lambda) = 0, \quad (A.7)$$

where

$$K(\lambda) = 3\beta_1^2(\lambda) + 2d_1(\lambda)\beta_1(\lambda) + d_2(\lambda) - 3\beta_2^2(\lambda),$$
$$L(\lambda) = 6\beta_1(\lambda)\beta_2(\lambda) + 2d_1(\lambda)\beta_2(\lambda),$$
$$M(\lambda) = \beta_1^2(\lambda)d_1'(\lambda) + d_2'(\lambda)\beta_1(\lambda) + d_3'(\lambda) - d_1'(\lambda)\beta_2^2(\lambda),$$
$$N(\lambda) = 2\beta_1(\lambda)\beta_2(\lambda)d_1'(\lambda) + d_2'(\lambda)\beta_2(\lambda).$$

Since $L(\lambda_{cr})N(\lambda_{cr}) + K(\lambda_{cr})M(\lambda_{cr}) \neq 0$, we have

$$Re\left[\frac{d\mu_j}{d\lambda}\right]_{\lambda=\lambda_{cr}} = \frac{LN+KM}{K^2+L^2}|_{\lambda=\lambda_{cr}} \neq 0$$

and

$$\mu_3(\lambda_{cr}) = -d_1(\lambda_{cr}) \neq 0.$$

The stability and the direction of bifurcation is given in Appendix B. These results are obtained by applying the algorithm due to Hassard et al. (1981), which depends upon the centre manifold theorem.

Appendix B. Stability of bifurcating limit cycle

We have already mentioned that we shall use the centre manifold theorem to investigate the stability of the limit cycles arising from Hopf bifurcation. It is worthwhile to mention that the centre manifold theorem is a powerful device for reducing the dimension of a system of differential equations in the vicinity of an equilibrium (for mathematical details and applications of the theorem, see, Guckenheimer and Holmes, 1983; Carr, 1981).

For the present system, given by Eq. (3), we find that the variational matrix V_* [see Eq. (A.1)] has real negative eigenvalue and a pair of purely imaginary eigenvalues at Hopf bifurcation. We may therefore analyse this system on a two-dimensional centre manifold. The flow transverse to the centre manifold is relatively simple, i.e., exponentially contracting.

To describe the centre manifold and analyse the flow therein, we first translate the origin of the coordinate system to the equilibrium (S^*, I^*, P^*) by writing

$$\overline{S} = S - S^*, \quad \overline{I} = I - I^*, \quad \overline{P} = P - P^*. \quad (B.1)$$

Then Eq. (3) can be written in the form

$$\frac{\mathrm{d}}{\mathrm{d}t}\begin{pmatrix}\overline{S}\\ \overline{I}\\ \overline{P}\end{pmatrix} = V_*\begin{pmatrix}\overline{S}\\ \overline{I}\\ \overline{P}\end{pmatrix} + \begin{pmatrix}h_1\\ h_2\\ h_3\end{pmatrix}. \tag{B.2}$$

Here the variational matrix V_* is given by Eq. (8) and the nonlinear terms are

$$h_1 = -b\overline{S}^2 - c\overline{P}\quad \overline{S} - \lambda\overline{I}\quad \overline{S},$$
$$h_2 = \lambda\overline{S}\quad \overline{I} - k\overline{P}\quad \overline{I},$$
$$h_3 = e\overline{P}\quad \overline{S} - k_1\overline{I}\quad \overline{P}.$$

At Hopf bifurcation, Eq. (A.3) holds and the eigenvalues of V_* are $\mu_1 = \alpha$ and $\mu_{2,3} = \pm \mathrm{i}w$, where $\alpha = -bS^*$,

$$w = \sqrt{kk_1P^*I^* + \lambda^2 I^*S^* + ceP^*S^*}. \tag{B.3}$$

If the eigenvector of V_* associated with μ_1 is W_1 and the eigenvectors corresponding to $\mu_{2,3}$ are $W_2 \pm \mathrm{i}W_3$ (W_1, W_2 and W_3 real), then it can be shown that the matrix $R = (W_3, W_2, W_1)$ is non-singular. Furthermore

$$R^{-1}V_*R = \begin{pmatrix}0 & -w & 0\\ w & 0 & 0\\ 0 & 0 & \alpha\end{pmatrix}. \tag{B.4}$$

We find that

$$R = \begin{bmatrix} wcS^* & -\lambda kS^*I^* & -\lambda kS^*I^* + c\alpha S^*\\ wkI^* & \lambda cS^*I^* + bkS^*I^* & c\lambda S^*I^* + kI^*(bS^* + \alpha)\\ -wcS^* & -w^2 - \lambda^2 S^*I^* & -\alpha(bS^* + \alpha) - \lambda^2 S^*I^*\end{bmatrix} \tag{B.5}$$

and

$$Q = R^{-1} = \frac{1}{A_1}\begin{bmatrix} q_{11} & q_{12} & q_{13}\\ q_{21} & q_{22} & q_{23}\\ q_{31} & q_{32} & q_{33}\end{bmatrix}, \tag{B.6}$$

where

$$q_{11} = I^*[\alpha bc\lambda S^{*^2} + \alpha b^2 kS^{*^2} + \alpha^2 c\lambda S^* + \alpha^2 bkS^* + w^2(c\lambda S^* + kbS^* + \alpha k) - \lambda^2 \alpha kS^*I^*],$$

$$q_{12} = \lambda S^*I^*(\alpha bkS^* + \alpha^2 k + \alpha\lambda cS^* + kw^2) - c\alpha w^2 S^*,$$

$$q_{13} = \alpha kS^*I^*(k\lambda I^* + c^2\lambda S^* + bcS^*),$$

$$q_{21} = -kwI^*(\alpha^2 + \lambda^2 S^*I^*) + bwS^{*^2}I^*(c\lambda + bk),$$

$$q_{22} = wcS^*(\alpha^2 + \lambda^2 S^*I^*) + wb\lambda kS^{*^2}I^*,$$

$$q_{23} = wcS^{*^2}I^*(c\lambda + bk) + \lambda wk^2 S^*I^{*^2},$$

$$q_{31} = wkI^*(\lambda^2 S^*I^* - w^2) - wbS^{*^2}I^*(c\lambda + bk),$$

$$q_{32} = wcS^*(w^2 - \lambda^2 S^*I^*) - \lambda k^2 wS^*I^{*^2},$$

$$q_{33} = -wcS^{*^2}I^*(c\lambda + bk) - \lambda k^2 wS^*I^{*^2}$$

and

$$A_1 = w(\alpha^2 + w^2)S^*I^*(\lambda c^2 S^* + bckS^* + \lambda k^2 I^*).$$

We now use the linear transformation

$$\begin{pmatrix}\overline{S}\\ \overline{I}\\ \overline{P}\end{pmatrix} = R\begin{pmatrix}I_1\\ I_2\\ I_3\end{pmatrix}, \tag{B.7}$$

which can be written as

$$\overline{\overline{Z}} = RW, \quad W = R^{-1}\overline{\overline{Z}}, \tag{B.8}$$

where $\overline{\overline{Z}} = (\overline{S}, \overline{I}, \overline{P})^{\mathrm{T}}$ and R is given by (B.5).

Substituting (B.8) into (B.2) gives $\frac{\mathrm{d}}{\mathrm{d}t}(RW) = V_*RW + F_1(RW)$ where, $F(\overline{\overline{Z}}) = (h_1, h_2, h_3)^{\mathrm{T}}$ which implies that

$$\frac{\mathrm{d}W}{\mathrm{d}t}(R^{-1}V_*R)W + R^{-1}F_1(RW), \tag{B.9}$$

where $W = (I_1, I_2, I_3)^{\mathrm{T}}$ and $R^{-1}V_*R$ is a constant matrix given by (B.4).

Now we can write (B.9) in the following manner:

$$\dot{x} = Ax + F_1(x, y),$$
$$\dot{y} = By + G_1(x, y), \tag{B.10}$$

where $x = (I_1, I_2)^{\mathrm{T}}$, $y = (I_3)$, A and B are the constant matrices

$$A = \begin{pmatrix}0 & -w\\ w & o\end{pmatrix}, \quad B = (\alpha) \tag{B.11}$$

and F_1 and G_1 are both C^2 functions. System (B.9) can now be written as

$$\frac{\mathrm{d}}{\mathrm{d}t}\begin{pmatrix}I_1\\ I_2\\ I_3\end{pmatrix} = \begin{pmatrix}0 & -w & o\\ w & 0 & 0\\ 0 & 0 & \alpha\end{pmatrix}\begin{pmatrix}I_1\\ I_2\\ I_3\end{pmatrix} + Q\begin{pmatrix}h_1\\ h_2\\ h_3\end{pmatrix}. \tag{B.12}$$

We now use the following two theorems.

Theorem 3. *System* (B.12) *has a local centre manifold* $y = \psi(x), x < \delta$ *where* ψ *is* C^2. *The function* $\psi(x)$ *can be approximated arbitrarily closely as a Taylor series as proved by the following theorem.*

Theorem 4. *Let* $\phi : S^n \to S^m$ *be* C^1 *in a neighbourhood of the origin,* $\phi(0) = 0, \phi'(0) = 0$ *and* $M\phi(x) = O(|x|^p)$ *as* $x \to 0$ *where*

$$M\phi(x) = \phi'(x)[Bx + G_1(x, \phi(x))] - A\phi(x) - F_1(x, \phi(x))$$

and $p > 1$. *Then* $\psi(x) = \phi(x) + O(|x|^p)$ *as* $x \to 0$.

Hence by following the result of Theorem 4 in the present case the centre manifold up to a quadratic

approximation, can be described by

$$I_3 = \psi(I_1, I_2) = \frac{1}{2}(b_{11}I_1^2 + 2b_{12}I_1I_2 + b_{22}I_2^2) + \text{h.o.t.} \tag{B.13}$$

where h.o.t. stands for higher-order terms.

Then it follows that:

$$\frac{dI_3}{dt} = \left(\frac{\delta\psi}{\delta I_1}\ \frac{\delta\psi}{\delta I_2}\right)\begin{pmatrix}\frac{dI_1}{dt}\\ \frac{dI_2}{dt}\end{pmatrix}, \tag{B.14}$$

which leads to

$$\begin{aligned}
&(b_{11}I_1 + b_{12}I_2 \quad b_{12}I_1 + b_{22}I_2)\begin{pmatrix}0 & -w\\ w & 0\end{pmatrix}\begin{pmatrix}I_1\\ I_2\end{pmatrix}\\
&\quad = I_1^2\Big[\frac{\alpha}{2}b_{11} - q_{31}bp_{11}^2 - q_{31}cp_{11}p_{31} - q_{31}\lambda p_{11}p_{21}\\
&\qquad + q_{32}\lambda p_{11}p_{21} - kq_{32}p_{21}p_{31}\\
&\qquad + eq_{33}p_{31}p_{11} + k_1q_{33}p_{21}p_{31}\Big]\\
&\qquad + I_1I_2[\alpha b_{12} - 2bq_{31}p_{11}p_{12}\\
&\qquad - cq_{31}(p_{11}p_{32} + p_{21}p_{12})\\
&\qquad - \lambda q_{31}(p_{11}p_{22} + p_{12}p_{21})\\
&\qquad + \lambda q_{32}(p_{11}p_{22} + p_{12}p_{21})\\
&\qquad - kq_{32}(p_{21}p_{32} + p_{31}p_{22})\\
&\qquad + eq_{33}(p_{31}p_{12} + p_{11}p_{32})\\
&\qquad + k_1q_{33}(p_{21}p_{32} + p_{22}p_{31})]\\
&\qquad + I_2^2\Big[\frac{\alpha}{2}b_{22} - bq_{31}p_{12}^2 - cq_{31}p_{12}p_{22} - \lambda q_{31}p_{12}p_{22}\\
&\qquad + \lambda q_{32}p_{12}p_{22} - kq_{32}p_{22}p_{32}\\
&\qquad + eq_{33}p_{32}p_{12} + k_1q_{33}p_{22}p_{32}\Big].
\end{aligned} \tag{B.15}$$

Comparing the coefficients of the terms with I_1^2, I_1I_2 and I_2^2 we obtain a system of linear equations for b_{11}, b_{12} and b_{22}

$$\begin{pmatrix}-\alpha/2 & w & 0\\ -w & -\alpha & w\\ 0 & -w & -\alpha/2\end{pmatrix}\begin{pmatrix}b_{11}\\ b_{12}\\ b_{22}\end{pmatrix} = \begin{pmatrix}Q_1\\ Q_2\\ Q_3\end{pmatrix} \tag{B.16}$$

where

$$\begin{aligned}
Q_1 = &- bq_{31}p_{11}^2 - cq_{31}p_{11}p_{31} - \lambda q_{31}p_{11}p_{21} + \lambda q_{32}p_{11}p_{21}\\
&- kq_{32}p_{21}p_{31} + eq_{33}p_{31}p_{11} + k_1q_{33}p_{21}p_{31}
\end{aligned}$$

$$\begin{aligned}
Q_2 = &- 2bq_{31}p_{11}p_{12} - cq_{31}(p_{11}p_{32} + p_{21}p_{12})\\
&- \lambda q_{31}(p_{11}p_{22} + p_{12}p_{21}) + \lambda q_{32}(p_{11}p_{22} + p_{12}p_{21})\\
&- kq_{32}(p_{21}p_{32} + p_{31}p_{22})\\
&+ eq_{33}(p_{31}p_{12} + p_{11}p_{32})\\
&+ k_1q_{33}(p_{21}p_{32} + p_{22}p_{31})
\end{aligned}$$

$$\begin{aligned}
Q_3 = &- bq_{31}p_{12}^2 - cq_{31}p_{12}p_{22} - \lambda q_{31}p_{12}p_{22}\\
&+ \lambda q_{32}p_{12}p_{22} - kq_{32}p_{22}p_{32}\\
&+ eq_{33}p_{32}p_{12} + k_1q_{33}p_{22}p_{32}.
\end{aligned}$$

We easily find that

$$\begin{aligned}
b_{11} &= -\frac{[w^2(Q_1 + Q_3) + \frac{\alpha}{2}(wQ_2 + Q_1\alpha)]}{(\frac{\alpha^3}{4} + w^2\alpha)}\\
b_{12} &= -\frac{[\frac{\alpha^2Q_2}{4} + \frac{w\alpha}{2}(Q_3 - Q_1)]}{(\frac{\alpha^3}{4} + w^2\alpha)}\\
b_{22} &= -\frac{[\frac{\alpha^2}{2}Q_3 - \frac{\alpha}{2}wQ_2 + w^2(Q_1 + Q_3)]}{(\frac{\alpha^3}{4} + w^2\alpha)}.
\end{aligned} \tag{B.17}$$

Then the flow on the centre manifold is governed by the two-dimensional system

$$\dot{x} = Ax + F(x, \psi(x)). \tag{B.18}$$

The next theorem, called the centre manifold theorem, tells us that (B.18) contains all the information needed to determine the asymptotic behaviours of solutions of (B.10).

Theorem 5. *Suppose that the zero solution of* (B.18) *is stable* (*asymptotically stable*) (*unstable*), *then the zero solution of* (B.10) *is stable* (*asymptotically stable*) (*unstable*).

(For the proofs of Theorems 3–5 see Carr, 1981).

In detailed form, (B.18) can be written as

$$\frac{d}{dt}\begin{pmatrix}I_1\\ I_2\end{pmatrix} = \begin{pmatrix}0 & -w\\ w & 0\end{pmatrix}\begin{pmatrix}I_1\\ I_2\end{pmatrix} + \begin{pmatrix}f_1\\ g_1\end{pmatrix} \tag{B.19}$$

where

$$f_1 = q_{11}h_1 + q_{12}h_2 + q_{13}h_3 + h.o.t$$

$$g_1 = q_{21}h_1 + q_{22}h_2 + q_{23}h_3 + h.o.t$$

with

$$\begin{aligned}
h_1 = &- \Big[b(p_{11}I_1 + p_{12}I_2)^2 + bp_{13}A(p_{11}I_1 + p_{12}I_2)\\
&+ c(p_{11}I_1 + p_{12}I_2)(p_{31}I_1 + p_{32}I_2)\\
&+ \frac{cAp_{33}}{2}(p_{11}I_1 + p_{12}I_2) + \frac{cAp_{13}}{2}(p_{31}I_1 + p_{32}I_2)\\
&+ \lambda(p_{11}I_1 + p_{12}I_2)(p_{21}I_1 + p_{22}I_2)\\
&+ \frac{\lambda Ap_{23}}{2}(p_{11}I_1 + p_{12}I_2)\\
&+ \frac{\lambda Ap_{13}}{2}(p_{21}I_1 + p_{22}I_2)\Big],
\end{aligned}$$

$$\begin{aligned}
h_2 = &\lambda(p_{11}I_1 + p_{12}I_2)(p_{21}I_1 + p_{22}I_2)\\
&+ \frac{\lambda Ap_{13}}{2}(p_{21}I_1 + p_{22}I_2)
\end{aligned}$$

$$+\frac{\lambda A p_{23}}{2}(p_{11}I_1+p_{12}I_2)$$
$$-k(p_{31}I_1+p_{32}I_2)(p_{21}I_1+p_{22}I_2)$$
$$-\frac{kAp_{33}}{2}(p_{21}I_1+p_{22}I_2)-\frac{kAp_{23}}{2}(p_{31}I_1+p_{32}I_2),$$

$$\begin{aligned}h_3 = &+e(p_{31}I_1+p_{32}I_2)(p_{11}I_1+p_{12}I_2)\\&+\frac{eAp_{13}}{2}(p_{31}I_1+p_{32}I_2)\\&+\frac{eAp_{33}}{2}(p_{11}I_1+p_{12}I_2)\\&+k_1(p_{21}I_1+p_{22}I_2)(p_{31}I_1+p_{32}I_2)\\&+\frac{k_1p_{23}A}{2}(p_{31}I_1+p_{32}I_2)+\frac{k_1Ap_{33}}{2}(p_{21}I_1+p_{22}I_2),\end{aligned}$$

$$A=b_{11}I_1^2+2b_{12}I_1I_2+b_{22}I_2^2.$$

The stability of the limit cycle arising from a Hopf bifurcation is determined by the sign of the quantity

$$\begin{aligned}B=&f_{111}+g_{112}+f_{122}+g_{222}+\frac{1}{w}[f_{12}(f_{11}+f_{22})\\&-g_{12}(g_{11}+g_{22})-f_{11}g_{11}+f_{22}g_{22}],\end{aligned}\tag{B.20}$$

where f_{ij} denotes the partial derivative $\partial^2 f/\partial I_i\,\partial I_j$ at the origin and the quantities with three subscripts represent third-order partial derivatives. For example, $g_{112}=\partial^3 g(0,0)/\partial I_1^2\partial I_2$ and so on. If $B<0$, the bifurcating limit cycle is stable and the Hopf bifurcation is called supercritical; if $B>0$, the limit cycle is unstable and we have a subcritical Hopf bifurcation. Calculations show that

$$\begin{aligned}f_{111} = &-q_{11}[6bp_{13}p_{11}b_{11}+3cp_{11}p_{33}b_{11}+3cp_{13}p_{31}b_{11}\\&+3\lambda p_{11}p_{23}b_{11}+3\lambda p_{13}p_{21}b_{11}]\\&+q_{12}[3\lambda p_{13}p_{21}b_{11}+3\lambda p_{11}p_{23}b_{11}-3kp_{21}p_{33}b_{11}\\&-3kp_{23}p_{31}b_{11}]\\&+q_{13}[3ep_{13}p_{31}b_{11}+3ep_{11}p_{33}b_{11}\\&+3k_1p_{23}p_{31}b_{11}+3k_1p_{33}p_{21}b_{11}],\end{aligned}\tag{B.21a}$$

$$\begin{aligned}g_{112} = &-q_{21}[2bp_{13}p_{12}b_{11}+4bp_{13}p_{11}b_{12}+cp_{12}p_{33}b_{11}\\&+2cp_{33}p_{11}b_{12}+cp_{13}p_{32}b_{11}+2cp_{13}b_{12}p_{31}\\&+\lambda b_{11}(p_{23}p_{12}+p_{13}p_{22})+2\lambda b_{12}(p_{23}p_{11}+p_{13}p_{21})]\\&+q_{22}[b_{11}(\lambda p_{13}p_{22}+\lambda p_{23}p_{12}-kp_{22}p_{33}-kp_{23}p_{32})\\&+2b_{12}(\lambda p_{13}p_{21}+\lambda p_{23}p_{11}-kp_{33}p_{21}-kp_{23}p_{31})]\\&+q_{23}[b_{11}(ep_{13}p_{32}+ep_{33}p_{12}+k_1p_{23}p_{32}\\&+k_1p_{33}p_{22})-2b_{12}(ep_{13}p_{31}+ep_{11}p_{33}\\&+k_1p_{23}p_{31}+k_1p_{21}p_{33})],\end{aligned}\tag{B.21b}$$

$$\begin{aligned}f_{122} = &-q_{11}[4bp_{12}p_{13}b_{12}+2bp_{13}p_{11}b_{22}+2cp_{33}p_{12}b_{12}\\&+cp_{33}p_{11}b_{22}+2cp_{13}p_{32}b_{12}+cp_{13}p_{31}b_{22}\\&+2\lambda b_{12}(p_{23}p_{12}+p_{13}p_{22})+\lambda b_{22}(p_{23}p_{11}+p_{13}p_{21})]\\&+q_{12}[2b_{12}(\lambda p_{13}p_{22}+\lambda p_{23}p_{12}-kp_{33}p_{22}-kp_{23}p_{32})\\&+b_{22}(\lambda p_{13}p_{21}+\lambda p_{23}p_{11}-kp_{33}p_{21}-kp_{23}p_{31})]\\&+q_{13}[2b_{12}(ep_{13}p_{32}+ep_{33}p_{12}+k_1p_{23}p_{32}\\&+k_1p_{33}p_{22})+b_{22}(ep_{13}p_{31}+ep_{33}p_{11}\\&+k_1p_{23}p_{31}+k_1p_{33}p_{21})],\end{aligned}\tag{B.21c}$$

$$\begin{aligned}g_{222} = &-3q_{21}[2bp_{12}p_{13}+cp_{33}p_{12}+cp_{13}p_{32}\\&+\lambda(p_{23}p_{12}+p_{13}p_{22})]b_{22}+3q_{22}b_{22}[\lambda p_{13}p_{22}\\&+\lambda p_{23}p_{12}-kp_{33}p_{22}-kp_{23}p_{32}]+3q_{23}b_{22}\\&\times[ep_{13}p_{32}+ep_{33}p_{12}+k_1p_{23}p_{32}+k_1p_{22}p_{33}],\end{aligned}\tag{B.21d}$$

$$\begin{aligned}f_{12} = &-q_{11}[2bp_{11}p_{12}+cp_{12}p_{31}+cp_{32}p_{11}+\lambda p_{11}p_{22}\\&+\lambda p_{12}p_{21}]\\&+q_{12}[\lambda p_{12}p_{21}+\lambda p_{11}p_{22}-kp_{32}p_{21}-kp_{31}p_{22}]\\&+q_{13}[ep_{32}p_{11}+ep_{31}p_{12}+k_1p_{22}p_{31}+k_1p_{21}p_{32}],\end{aligned}\tag{B.21e}$$

$$\begin{aligned}g_{12} = &-q_{21}[2bp_{11}p_{12}+cp_{12}p_{31}+cp_{32}p_{11}+\lambda p_{11}p_{22}\\&+\lambda p_{12}p_{21}]\\&+q_{22}[\lambda p_{12}p_{21}+\lambda p_{11}p_{22}-kp_{32}p_{21}-kp_{31}p_{22}]\\&+q_{23}[ep_{32}p_{11}+ep_{31}p_{12}+k_1p_{22}p_{31}+k_1p_{21}p_{32}],\end{aligned}\tag{B.21f}$$

$$\begin{aligned}f_{22} = &-2q_{11}p_{12}[bp_{12}+cp_{32}+\lambda p_{22}]\\&+2q_{12}p_{22}[\lambda p_{12}-kp_{32}]\\&+2q_{13}p_{32}[ep_{12}+k_1p_{22}],\end{aligned}\tag{B.21g}$$

$$\begin{aligned}g_{22} = &-2q_{21}p_{12}[bp_{12}+cp_{32}+\lambda p_{22}]\\&+2q_{22}p_{22}[\lambda p_{12}-kp_{32}]\\&+2q_{23}p_{32}[ep_{12}+k_1p_{22}],\end{aligned}\tag{B.21h}$$

$$\begin{aligned}f_{11} = &-2q_{11}p_{11}[bp_{11}+cp_{31}+\lambda p_{21}]\\&+2q_{12}p_{21}[\lambda p_{11}-kp_{31}]\\&+2q_{13}p_{31}[ep_{11}+k_1p_{21}],\end{aligned}\tag{B.21i}$$

$$\begin{aligned}g_{11} = &-2q_{21}p_{11}[bp_{11}+cp_{31}+\lambda p_{21}]\\&+2q_{22}p_{21}[\lambda p_{11}-kp_{31}]\\&+2q_{23}p_{31}[ep_{11}+k_1p_{21}].\end{aligned}\tag{B.21j}$$

The sign of B can be deduced by evaluating the various quantities in Eqs. (B.21) in terms of the system parameters b,c,λ,k,e and substituting the resulting expressions into Eq. (B.20).

References

Agusti, S., Duarte, C.M., Kalff, J., 1987. Algal cell size and the maximum density and biomass of phytoplankton. Limnol. Occeangr. 32, 983–986.

Anderson, R.M., May, R.M., 1991. Infectious Diseases of Humans, Dynamics and Control. Oxford University Press, Oxford.

Arme, C., Owen, R.W., 1967. Infections of the three-spined stickleback, *Gasterostens acnleatus L.*, with the plerocercoid larvae of *Schiotocephalus solidus* (Muller, 1776), with special reference to pathological effects. Parasitology 57, 301–314.

Beltrami, E., Carroll, T.O., 1994. Modelling the role of viral disease in recurrent phytoplankton blooms. J. Math. Biol. 32, 857–863.

Bergh, O., Borsheim, K.Y., Bratbak, G., heldal, M., 1989. High abundance of viruses found in aquatic environments. Nature 340, 467–468.

Bratbak, G., Levasseur, M., Michand, S., Contin, G., Fernandez, E., Heldel, M., 1995. Viral activity in relation to Emiliania huxleyi blooms: a mechanism of DMSP release. Mar. Ecol. Progr. Ser. 128, 133–142.

Brussaard, C.P.D., Gast, G.J., van Duyl, F.C., Riegman, R., 1996. Impact of phytoplankton bloom magnitude on a pelagic microbial food web. Mar. Ecol. Prog. Ser. 144, 211–221.

Carr, J., 1981. Applications of Center Manifold Theory. Springer, New York.

Chattopadhyay, J., Arino, O., 1999. A predator prey model with disease in the prey. Nonlinear Anal. 36, 747–766.

Chattopadhyay, J., Pal, S. 2002. Viral infection of phytoplankton zooplankton system—a mathematical modelling. Ecol. Model.

Chattopadhyay, J., Ghosal, G., Chaudhuri, K.S., 1999. Nonselective harvesting of a predator–prey community with infected prey. Korean J. Computatl. Appld. Math. 6, 601–616.

De Jong, M.C.M., Diekmann, O., Heesterbeek, J.A.P., 1994. How does infection transmission depend on population size?. In: Mollison, D. (Ed.), Epidemic Models, Their Structure and Relation to Data. Cambridge University Press, Cambridge.

Ebert, U., Arrayas, M., Temme, N., Sommeijer, B., Huisman, J., 2001. Critical conditions for phytoplankton blooms. Bull. Math. Biol. 63, 1095–1124.

Edelstein-Keshet, L., 1988. Mathematical Models in Biology. Random House, New York, pp. 78–83.

Edwards, A.M., Brindley, J., 1996. Oscillatory behaviour in a three-component plankton population model. Dynam. Stability Syst. 11, 347–370.

Freedman, H.I., 1990. A model of predator-prey dynamics as modified by the action of parasite. Math. Biosci. 99, 143–155.

Guckenheimer, J., Holmes, P.J., 1983. Nonlinear Oscillations, Dynamical Systems and Bifurcation of Vector Fields. Springer, New York.

Hadeler, K.P., Freedman, H.I., 1989. Predator–prey population with parasite infection. J. Math. Biol. 27, 609–631.

Hamilton, W.D., Axelrod, R., Tanese, R., 1990. Sexual reproduction as an adaptation to resist parasite: a review. Proc. Natl Acad. Sci. USA 87, 3566–3573.

Hassard, B.D., Kazarinoff, Y.H., Wan, Y.H., 1981. Theory and Applications of Hopf-bifurcation. Cambridge University Press, Cambridge.

Holmes, J.C., Bethel, W.M., 1972. Modification of intermediate host behaviour by parasites. in: Cunning, E.V., Wright, C.A. (Eds.), Behavioural Aspects of Parasites Transmissions. Zool. J. Linn. Soc. 51 (Suppl. 1), 123–149.

Huisman, J.P., Van Oostveen, Weissing, F.J., 1999. Critical depth and critical turbulence: two different mechanisms for the development of phytoplankton blooms. Limnol. Oceanogr. 44, 1781–1788.

Inoue, M., Kamifukumoto, H., 1984. Scenarios leading to chaos in a forced Lotka Volterra model. Prog. Theor. Phys. 71, 930–937.

Kermack, W.O., McKendrick, A.G., 1927. Contributions to the mathematical theory of epidemics. Proc. R. Soc. London Series A 115, 700–721.

Lafferty, K.D., Morris, A.K., 1996. Altered behaviour of parasitized kill fish increases susceptibility to predation by bird final hosts. Ecology 77, 1390–1397.

McAdams, H.H., Arkin, A., 1999. It's a noisy business. Trends Genet. 15, 65–69.

Murray, J.D., 1989. Mathematical Biology. Springer, New York.

Nagasaki, K., Yamaguchi, M., 1997. Isolation of a virus infectious to the harmful blooms causing microalga Heterosigma akashiwo (raphidophyceae). Aquat. Microbiol. Ecol. 13, 135–140.

Peduzzi, P., Weinbauer, M.G., 1993. Effect of concentrating the virus-rich 2–200 nm size fraction of seawater on the formation of algal flocs (marine snow). Limnol. Oceanogr. 38, 1562–1565.

Pitchford, J.W., Brindley, J., 1998. Intratrophic predation in simple predator-prey models. Bull. Math. Biol. 60, 937–953.

Platt, T., Bird, D.F., Sathyendranath, S., 1991. Critical depth and marine primary production. Proc. Roy. Soc. London B 246, 205–217.

Platt, T., Fuentes-Yaco, C., Frank, K.T., 2003. Spring algal bloom and larval fish survival. Nature 423, 398–399.

Reisser, W., 1993. Viruses and virus-like particles of freshwater and marine eukaryotic algae — a review. Arch. Protistenkunde 143, 257–265.

Rinaldi, S., Muratori, S., Kuznetsov, Y., 1993. Multiple attractors, catastrophe and chaos in seasonally perturbed predator-prey communities. Bull. Math. Biol. 55, 15–35.

Rosenzweig, M.L., MacArthur, R.H., 1963. Graphical representation and stability conditions of predator–prey interactions. Amer. Nat. 97, 209–223.

Smayda, T.J., 1997a. What is a bloom? A commentary. Limnol. Occeanogr. 42 (5 Part 2), 1132–1136.

Smayda, T.J., 1997b. Harmful phytoplankton blooms: their ecophysiology and general relevance to phytoplankton blooms in the sea. Limnol. Occeanogr. 42, 1137–1153.

Steele, J.H., Henderson, E.W., 1993. The significance of interannual variability. In: Evans, G.T., Fasham, M.J.R. (Eds.), Towards a Model of Ocean Biogeochemical Processes. Springer, Berlin, pp. 237–260.

Suttle, C.A., Chan, A.M., 1993. Marine cyanophages infecting oceanic and coastal strains of Synechococcus: abundance, morphology, cross-infectivity and growth characteristics. Mar. Ecol. Prog. Ser. 92, 99–109.

Suttle, C., Charm, A., Cottrell, M., 1990. Infection of phytoplankton by viruses and reduction of primary productivity. Nature 347, 467–469.

Suttle, C.A., Chan, A.M., Chen, F., Garza, D.R., 1993. Cynophages and sunlight: a paradox. In: Guerrero, R., Pedros-Alio, C. (Eds.), Trends in Microbial Ecology. Spanish Society for Microbiology, Barcelona.

Tont, S., 1976. Short-period climatic fluctuations: effects on diatom biomass. Science 194, 942–944.

Truscott, J.E., Brindley, J., 1994. Ocean plankton populations as excitable media. Bull. Math. Biol. 56, 981–998.

Uhlig, G., Sahling, G., 1992. Long-term studies on *Noctilucascintillans* in the German bight. Neth. J. Sea Res. 25, 101–112.

van Etten, J.L., Lane, L.C., Meints, R.H., 1991. Viruses and virus like particles of eukaryotic algae. Microbiol. Rev. 55, 586–620.

Venturino, E., 1995. Epidemics in predator-prey models: disease in the prey. In: Arino, O., Axelrod, D., Kimmel, M., Langlais, M. (Eds.), Mathematical Population Dynamics: Analysis of Heterogeneity, vol. 1, pp. 381–393.

Weissing, F.J., Huisman, J., 1994. Growth and competition in a light gradient. J. Theor. Biol. 168, 323–336.

Williams, H.H., 1967. Helminth diseases of fish. Helminth Abstr. 36, 261–295.

Xiao, Y., Chen, L., 2001. Modelling and analysis of a predator–prey model with disease in the prey. Math Biosci. 171, 59–82.